JGR Atmospheres

RESEARCH ARTICLE
10.1029/2022JD037485

A New Instrument for Balloon-Borne *In Situ* Aerosol Size Distribution Measurements, the Continuation of a 50 Year Record of Stratospheric Aerosols Measurements

Lars E. Kalnajs[1] **and Terry Deshler**[1]

[1]Laboratory for Atmospheric and Space Physics, University of Colorado Boulder, Boulder, CO, USA

Key Points:

- A new balloon-borne optical particle counter has been developed to measure stratospheric aerosol size distributions
- The instrument is being used to continue a 50-yr *in situ* measurement record of the stratospheric aerosol layer
- Comparisons with the SAGE III/International Space Station satellite instrument have shown generally good agreement from the tropopause to 25 km

Correspondence to:
L. E. Kalnajs,
kalnajs@colorado.edu

Citation:
Kalnajs, L. E., & Deshler, T. (2022). A new instrument for balloon-borne *in situ* aerosol size distribution measurements, the continuation of a 50 year record of stratospheric aerosols measurements. *Journal of Geophysical Research: Atmospheres*, *127*, e2022JD037485. https://doi.org/10.1029/2022JD037485

Received 11 JUL 2022
Accepted 29 NOV 2022

Author Contributions:
Conceptualization: Lars E. Kalnajs, Terry Deshler
Data curation: Terry Deshler
Formal analysis: Lars E. Kalnajs, Terry Deshler
Funding acquisition: Lars E. Kalnajs, Terry Deshler
Investigation: Lars E. Kalnajs, Terry Deshler
Methodology: Terry Deshler
Project Administration: Lars E. Kalnajs, Terry Deshler
Software: Lars E. Kalnajs
Supervision: Lars E. Kalnajs, Terry Deshler

Abstract Profiles of stratospheric aerosol size distributions have been measured using balloon-borne *in situ* optical particle counters, from Laramie, Wyoming (41°N) since 1971. In 2019, this measurement record transitioned to the Laboratory for Atmospheric and Space Physics (LASP) in Boulder, Colorado (40°N). The new LASP Optical Particle Counter (LOPC), the fourth generation of instruments used for this record, is smaller and lighter (2 kg) than prior instruments, measures aerosols with diameters ≥0.3–30 μm in up to 450 size bins, with a flow rate of 20 L min^{-1}. The improved size resolution enables the complete measurement of size distributions, and calculation of aerosol extinction without fitting *a priori* distribution shapes. The higher flow provides the sensitivity required to measure super-micron particles in the stratosphere. The LOPC has been validated against prior Wyoming OPCs, through joint flights, laboratory comparisons, and statistical comparisons with the Wyoming record. The agreement between instruments is generally within the measurement uncertainty of ±10%–20% in sizing and ±10% in concentration, and within ±40% for calculated aerosol moments. The record is being continued with balloon soundings every 2 months from Colorado, coordinated with measurements of aerosol extinction from the SAGE III instrument on the International Space Station. Comparisons of aerosol extinction from the remote and *in situ* platforms have shown good agreement in the stratosphere, particularly for wavelengths <755 nm and altitudes <25 km. For extinction wavelengths ≥1,021 nm and altitudes above 25 km SAGE III/International Space Station extinction has a low bias relative to the *in situ* measurements, yet still within the ±40% uncertainty.

Plain Language Summary Small particles in the upper levels of the atmosphere play an important role in climate and chemistry of the atmosphere. These small aerosol particles have been measured using optical particle counters (OPCs) on high altitude balloons since 1971 from Laramie, Wyoming. Recently, a new OPC has been developed at the Laboratory for Atmospheric and Space Physics in Boulder, Colorado, and this long-term record is being continued from Boulder using the new instrumentation. The new instrument is smaller, lighter, and cheaper than the previous instruments, but the performance of the new instrument has been validated against the prior generation of instruments. The new instrument is being used to validate measurements of aerosol extinction from the SAGE III instrument on the International Space Station (ISS). These comparisons confirm that the aerosol extinction measurements from SAGE III/ISS are in good agreement with the balloon born record.

1. Introduction

The globally distributed stratospheric aerosol is a constant but highly variable component of the Earth's atmosphere. They impact climate through their albedo as well as ozone through heterogeneous chemistry. For these reasons, they must be considered in global climate predictions from global climate-chemistry models, and there are a host of measurement platforms to characterize these aerosol. Their optical properties have been measured passively from satellites using solar occultation, since the late 1970s, and limb scattering, since the early 2000s (Bourassa et al., 2007; Llewellyn et al., 2004; McCormick et al., 1979; Russell et al., 1981; Thomason et al., 2018). Active satellite measurements of backscatter began in the mid-2000s (Vernier et al., 2011), while surface based lidar measurements have been completed regularly at a handful of locations since the mid-1970s (Barnes & Hofmann, 1997; Jäger, 2005). The first measurements, however, were completed using *in situ* instruments deployed on balloons (Junge et al., 1961) and aircraft (Junge & Manson, 1961) leading to an understanding of the worldwide distribution of the aerosol. Since that time *in situ* measurements have continued on a few aircraft (Reeves et al., 2008) and at a few ballooning locations since the early 1970s (Deshler et al., 2003; Hofmann &

Validation: Lars E. Kalnajs, Terry Deshler
Writing – original draft: Lars E. Kalnajs
Writing – review & editing: Terry Deshler

Rosen, 1981). In contrast to the satellite and lidar measurements, which provide extinction or backscatter, the *in situ* measurements provide size distributions, and thus the only direct path for deriving the microphysical parameters required by the global models such as aerosol surface area, volume, and cross section. Even though the *in situ* instruments measure size distributions their fundamental measurements are still, for the most part, based on optical properties of the aerosol as they use Mie scattering to size the particles, hence their characterization as optical particle counters (OPCs).

The *in situ* aerosol measurement record has relied on a variety of instruments from impaction grids and counting by hand (Bigg et al., 1970) to OPCs, with the latter dominating the measurements since the 1970s. The longest continuous *in situ* measurement record has been located in Laramie, Wyoming, with quasi-monthly sounding profiles completed from 1971 to 2019 (Deshler et al., 2003, 2019; Hofmann & Rosen, 1981, 1987; Hofmann et al., 1975). Maintaining any 50-yr measurement record requires a host of instruments. The first OPCs were two channel instruments, reporting particles larger than 0.3 and 0.5 μm diameter, with a flow rate of 1 L per minute developed in the 1960s (Rosen, 1964), deployed regularly beginning in 1971, and continuing into the early 1990s. Discovery of the ozone hole led to a modification of this instrument to a 10 L per minute instrument with size resolution from 0.3 to 20 μm to measure polar stratospheric clouds (Hofmann & Deshler, 1991). The third iteration was developed due to looming shortages in critical components and marked a shift from a white light-based forward scatter counter to a laser-based side scatter counter (Ward et al., 2014). Table 1 summarizes the characteristics of the balloon-borne OPCs which make up this 50-yr record. The latest iteration in this measurement record is to a new laser-based side scatter counter developed at the Laboratory for Atmospheric and Space Physics (LASP), the LASP OPC (LOPC), final row in Table 1. The characteristics of this instrument, its description, validation, and application are the subjects of this paper.

Balloon-borne OPCs have long been used to provide *in situ* validation of remotely sensed aerosol extinction profiles. Size distribution profiles from Laramie, Wyoming, have previously been used for comparison with aerosol extinction profiles from SAM, SAGE II, HALOE, CLAES, and ISAMS (Hervig & Deshler, 2002; Massie et al., 1996; Russell et al., 1981, 1984). Here we describe the first comparisons of the recently released version 5.2 aerosol extinction profiles from SAGE III/International Space Station (ISS) solar occultations with balloon-borne *in situ* aerosol size distribution measurements using the new LOPC. The balloon flights were coordinated in time and space with nearby SAGE III/ISS aerosol extinction measurements. For this study we will concentrate on the 521, 755, and 1,021 nm aerosol extinction channels as these are very similar to the SAGE II 525 and 1,020 nm aerosol extinction channels, and to the OSIRIS 750 nm channel used in previous satellite and *in situ* comparisons. For these wavelengths, the bulk of the aerosol extinction is captured within the sizing limitations of the OPCs. *in situ* measurements were performed using both the last generation of University of Wyoming Laser Particle Counter (herein WLPC) (Ward et al., 2014) and the newly developed LOPC. Flights were performed from both Wyoming and Colorado.

The new LOPC is significantly smaller (10 × 15 × 30 cm), lighter (2 kg), and less expensive than the prior Wyoming legacy instruments, enabling more frequent launches using smaller balloons and thus tighter coordination with external requirements, for example, satellite overpasses and rapid response measurement of volcanic eruptions and wildfires. Furthermore, the LOPC has significantly higher sizing resolution, increasing the number of size bins from 8 (WLPC) to a native resolution of 450 bins for the LOPC. The increase in resolution has allowed for the direct determination of aerosol extinction without the need to fit an assumed size distribution to the number density measurements. In addition to providing *in situ* validation of SAGE III/ISS these measurements provide continuity with and extend the 50 yrs record of *in situ* stratospheric aerosol size distribution measurements begun in Laramie in 1971 (Deshler et al., 2006).

2. LOPC Instrument Description

The LOPC is conceptually similar to the prior generations of balloon-borne stratospheric OPCs including the original white light OPCs (Deshler et al., 2003; Rosen, 1964) as well as the more recent laser based WLPC (Ward et al., 2014). As with all OPCs the instrument determines the optical diameter of an aerosol particle by measuring the intensity of light scattered by a single particle and applying Mie theory to determine the optical diameter of the scattering particle, assuming an *a priori* refractive index.

Table 1
A Comparison of Optical Particle Counters Used Over the Past 50 Years From Wyoming and Colorado for In Situ Stratospheric Aerosol Size Distributions

Name/acronym	Years used	Diameter range (μm)	Number of sizes	Flow rate (LPM)	Scattering angle(s)	Light source	Weight (kg)	Reference
Dust	1971–2003	0.3–0.5	2	1	20–30	White light	5	Rosen, 1964
WOPC	1989–2013	0.38–20.0	8–12	10	35–45	White light	6	Deshler et al., 2003
WLPC	2008–2020	0.18–20.0	8	10	60–120	Laser 633 nm	5	Ward et al., 2014
LOPC	2019–	0.3–30.0	450	20	60–120	Laser 780 nm	2	This work

The LOPC is based on the Met One BT620 optical assembly which is capable of operating under the high flow rates required to maintain sensitivity in the stratosphere. From Met One we obtain customized optical heads, including the optics, laser, detector, and first stage of amplification. The optical layout is shown in Figure 1. A laser diode (laser power: 90 mW, wavelength: 780 nm) illuminates the instrument sample volume using beam shaping optics to produce a uniform rectangle or curtain of light approximately 6 mm across the air flow by 1 mm along the airflow. A 4.5 mm diameter intake nozzle introduces a stream of ambient air into the sample volume. The entire air stream is illuminated by the curtain of laser light immediately after the air leaves the nozzle. Light scattered from the aerosol within the air stream is collected by focusing optics with a 60° solid collection angle, centered at 90° to both the laser beam and the air stream. The collection optics focuses the scattered light onto a photodiode which converts the pulses of scattered light into an electrical signal. These analog pulses are processed by a pulse shaper that normalizes the pulse width to a 6 μs wide Gaussian pulse, while maintaining the pulse height. The rest of the electronics, including pulse height analysis, flow system, and mechanics were developed at LASP.

In contrast to prior generations of instruments where these electrical pulses were categorized using a limited (2–12) number of hardware discriminators, the LOPC directly digitizes the pulses using two parallel high speed 10-bit analog to digital converters (ADCs). The range of pulse heights from particles with diameters between 0.3 and 30 μm spans three orders of magnitude. To provide sufficient resolution to digitize 0.005–7 V pulses, two parallel ADCs, with a factor of 5 difference in analog gain, simultaneously sample the analog signal. Digitization of a pulse is initiated by a hardware comparator once the signal from the photodiode exceeds a threshold value that is set during calibration. Each digitized pulse from the ADCs is processed in real time to measure both pulse height and width. If the pulse width is within acceptable limits, the corresponding pulse height bin, in an array of bins representing all possible pulse heights, is incremented by one. Instances of coincident counting, where two

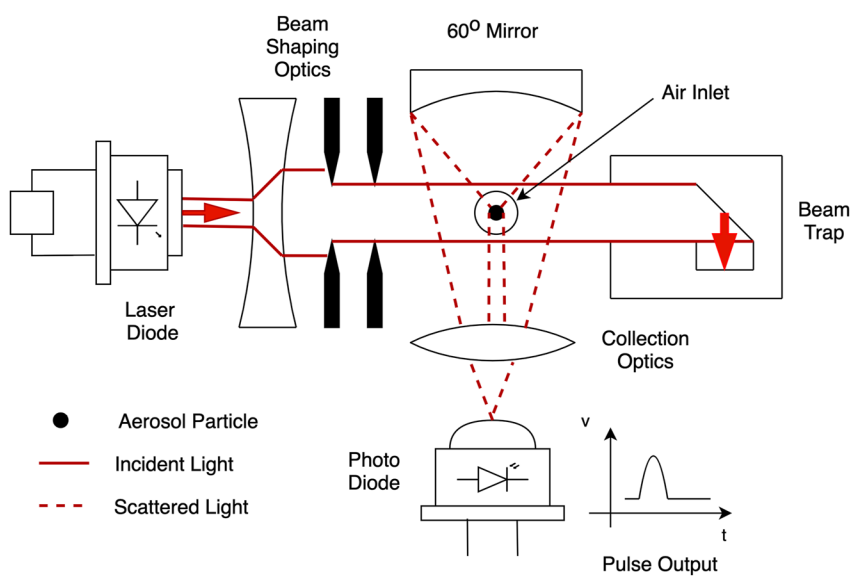

Figure 1. Schematic diagram of the LASP Optical Particle Counter (LOPC) optical system. Air flow is perpendicular to the page.

particles pass through the beam at the same time, will typically be rejected by the pulse height analyzer due to excessive pulse width. This pulse height array is accumulated for 2 s before being stored locally and telemetered to the ground at a reduced resolution. The raw data is recorded in 1,024 bins for each gain stage, yielding 2,048 channels; however, there is overlap between gain stages and some noise in the processing, thus the effective native resolution is approximately 450 bins. The lower particle size limit of the instrument is determined by the corresponding pulse height relative to the noise threshold in the detector and electronics. The pulse height is proportional to the intensity of the illuminating laser light. The laser diode used in the LOPC is smaller and lighter than previous instruments, but provides less intense illumination than the intra-cavity gas laser used in the WLPC, thus the minimum detectable particle size has increased on the LOPC. Laboratory experiments using polystyrene latex (PSL) spheres have shown sensitivity to particles of diameter greater than 0.25 μm. However, the data is publicly reported with a lower most size of 0.3 μm as sizes of particles below 0.3 μm have a counting efficiency of less than 1, and higher sizing uncertainty, as the pulse heights are closer to the noise floor of the electronics.

Flow through the instrument is maintained at 20 L min^{-1} using a pair of graphite rotary vane, constant volume, pumps operating in parallel (Thomas G-09 Series). The volume of air moved by the pump is primarily dependent on rotational speed and is largely independent of pressure or air density. The speed of the pumps is adjusted in the laboratory to provide a volume flow of 20 L min^{-1}, and is then controlled to this speed throughout the flight using a digital feedback scheme. Every 2 s, the drive voltage to each pump is momentarily interrupted for 1 ms, during this momentary interruption the voltage generated by the still spinning motor and pump rotor is measured, providing feedback to the instrument control system as to the pump rotation speed. The drive voltage to the pump is digitally controlled to maintain this pump speed feedback at a constant value. The volumetric flow is essentially constant as it passes through the pump head, but as the temperature of the pump head is higher than the ambient air temperature at the inlet, the flow is adjusted in post processing by the ratio of ambient to pump head temperature to yield the volume flow at the instrument inlet. The volume flow rate is twice the flow rate of the preceding WLPC, and is sensitive at 0.5 Hz to aerosol concentrations down to 10^{-4} cm^{-3}, sufficient to resolve super-micron particles in the mid-stratosphere, a unique capability for high flow rate balloon-borne OPCs.

The LOPC has an integrated GPS receiver allowing for standalone operation; however it is typically interfaced with an iMet-1-RSB or iMet-4-RSB radiosonde to provide state variables, pressure, temperature and relative humidity, and telemetry of aerosol data to the ground through the iMet X-Data protocol. The instrument is powered by a lithium polymer battery pack, and is capable of 5 hr of continuous measurements. At 2 kg, the LOPC is light enough to be flown on a rubber sounding balloon and the balloon system can be classified as a light balloon, exempting it from many of the air traffic regulations governing the prior generations of OPCs flown from Laramie, Wyoming.

2.1. LOPC Instrument Calibration

The raw data stored on the LOPC is the pulse height array, consisting of 2,048 bins. These bins are in two gain ranges, a high gain array for pulses with heights less than 1.0 V, corresponding to particles with a diameter of less than 2 μm, and a low gain array for pulses larger than 1.0 V. There is significant overlap between the arrays, so a stitch point around 0.5 V or 1 μm is chosen to append the two gain stages together and the repeated bins in the low gain stage are discarded. To reduce noise the arrays are further down sampled by a factor of 4, resulting in approximately 450 bins that are used for analysis. The bins in the high gain array (submicron particles) are a factor of 5 more closely spaced in pulse height than the bins in the low gain array (supermicron particles). Within each array, bins are spaced linearly with respect to pulse height, however due to the exponential increase in pulse height with diameter, bin spacing is quasi-logarithmic in diameter space. Bin widths range from 0.005 μm for diameters near 0.3 μm up to 0.1 μm for particles larger than 10 μm. The pulse height for each of these bins is converted to optical diameter using the Counter Response Function (CRF), the form of which is derived from Mie scattering. For the LOPC the CRF is given by Equation 1.

$$CRF(d) = \int_{60}^{120} \left(\frac{\lambda}{2\pi}\right)^2 \left[i_1(d, m, \lambda) + i_2(d, m, \lambda)\right]\ E(\lambda)\, d\theta, \tag{1}$$

where λ is the laser wavelength, 780 nm, $i_{1/2}$ are the Mie scattering coefficients for an aerosol of diameter, d, index of refraction, m, $E(\lambda)$ is the energy per unit area in the scattering region, and θ is the angle over which the scattered light, which at any scattering angle is not axially dependent, is collected. In contrast to CRFs for white light-based

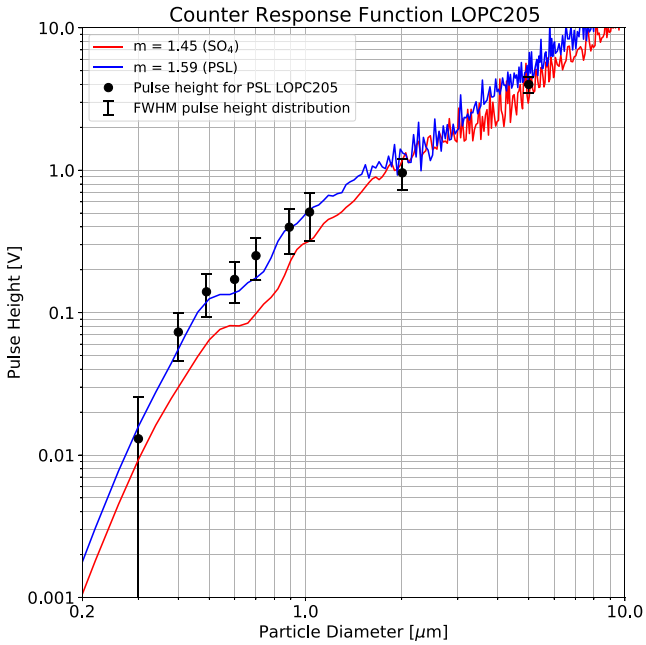

Figure 2. Calculated LASP Optical Particle Counter (LOPC) Counter Response Function for sulfate aerosol (red) and polystyrene latex (PSL) (blue). Solid circles show the median pulse height for eight sizes of PSL; error bars denote the full width half maximum (FWHM) pulse height distribution for each PSL size.

OPCs (Deshler et al., 2003; Pinnick et al., 1973) there is no integration over wavelength, nor over the light focusing optics, required for a laser instrument. The CRF for the LOPC is shown in Figure 2 for particles between 0.3 and 10 μm and for two indices of refraction, 1.59 in blue representing PSL spheres and 1.45 in red, representing sulfate stratospheric aerosol. Based on the laser wavelength, optical geometry, and minimum detectable pulse height, the counter response is monotonically increasing from 0.25 to 2.0 μm particle diameter. From 2.0 to 30.0 μm the response, while still generally increasing, is no longer strictly monotonic due to Mie oscillations, thus the uncertainty in particle sizing is greater for particles over 2.0 μm.

While the shape of the CRF is defined by Mie scattering, given the optical environment of the particle, the intensity of the laser, sensitivity of the detector, and precise gain on the two ADCs is not necessarily constant between LOPC instruments. Furthermore, the Mie curve is a complex mathematical relationship, particularly above 2.0 μm. As a result, each instrument is individually calibrated using monodisperse PSL. Eight sizes of PSL ranging from 0.3 to 2.0 μm are used and the resulting pulse height for each PSL is recorded in the laboratory. An example of the response for a typical LOPC (serial number LOPC205) to monodisperse PSL is shown in Figure 2. For each size of PSL, the peak in the pulse height distribution is marked, as well as the full width half maximum for the distribution of pulse heights produced for each size of PSL. The width of the OPC response to monodisperse aerosol is discussed in some detail by Deshler et al. (2003, 2019) among others. This distribution is driven by several factors. The intensity of laser light illuminating the particles, as they pass through the beam, will vary some over the sensing region, particularly for high flow rate instruments where the laser beam is expanded to cover a larger detection volume. Thus, there may be small position-dependent variations in particle illumination in the beam, along with small position-dependent variations in the Mie scattering. There is inherent electrical noise in the analog photodiode, pulse shaper, and digitization system. This has a more significant impact on smaller particles, which produce small pulse heights. Finally, there is some width to the distribution of monodisperse aerosol. Based on this pulse distribution width, the 2σ sizing accuracy of the instrument is estimated to be ±10% for particles smaller than 2 μm, increasing to ±20% for particles greater than 2 μm due to the additional uncertainty introduced by the non-monotonic response for larger particles.

The PSL used for calibration have a refractive index of 1.59 at the laser wavelength of 780 nm (Ma et al., 2003) whereas the mean refractive index for the primarily sulfate stratospheric aerosol is approximately 1.45. Using the CRF for the LOPC and refractive indices of 1.59 and 1.45, the PSL diameters can be converted to the diameter equivalent sulfate particle that would produce an equivalent pulse height in the LOPC. For example, a 0.4 μm PSL particle produces the same pulse height as a 0.48 μm sulfate aerosol. The Mie CRF for the instrument is not bijective and thus there is no inverse function to calculate diameter from pulse height. Thus, a piecewise curve fit is performed using three third order polynomials (a cubic spline) to define a mathematically tractable relationship between pulse height and diameter, which can then be used to determine a sulfate equivalent diameter for each of the 450 effective LOPC bins.

The LOPC has a uniquely high flow rate (20 L m^{-1}) relative to other OPCs for balloon-borne measurements, and about twice the flow of the prior high flow rate Wyoming instruments. For stratospheric aerosol, the low concentrations of aerosol lead to relatively infrequent detection of particles, and thus the uncertainty in particle counting is dominated by Poisson counting statistics for the large particles and is proportional to $N^{0.5}$, where N is the number of counts in an integration period. Since concentration, C, is $N/(dt\ FR)$ for integration time dt, and flowrate FR, the concentration uncertainty is given by $1/(C\ dt\ FR)^{0.5}$. For diameters larger than 0.3, 0.5, and 1.0 μm, typical nonvolcanic particle cumulative concentrations are on the order of 1.0, 0.1, and 0.01 cm^{-3}, respectively. With FR = 20 L min^{-1} (333 cm^3 s^{-1}), and dt = 2 s the concentration uncertainty is 4%, 12%, and 39% for concentrations of 1.0, 0.1, and 0.01 cm^{-3}. The high flow rate of the instrument can lead to issues with coincidence counting at higher particle concentrations. Based on the sensing volume (0.016 cm^3) coincidence

counting becomes significant at aerosol concentrations approaching 30 cm^{-3}, well above concentrations encountered in the stratosphere. With a typical balloon ascent rate of 5 m s^{-1} and a 2 s integration time, the effective vertical resolution of the measurement is 10 m.

3. Comparing the LOPC to Prior Generations of Wyoming OPC

The LOPC was developed as a successor to the series of balloon-borne OPCs that were developed at the University of Wyoming. The first of these instruments, the Wyoming Dust Sonde, a two-channel instrument with an incandescent white light source, was developed in the 1960s (Rosen, 1964) and was used for regular measurements of stratospheric aerosol beginning in 1971 (Hofmann et al., 1975). This instrument was superseded by an 8- to 12-channel white light instrument (WOPC) in 1989, that was flown until 2013 (Deshler et al., 2003, 2019). The last generation of Wyoming instruments is a laser particle counter (WLPC) using a He-Ne laser and reporting eight size channels (Ward et al., 2014). Each successive generation of particle counter provided improved measurement capabilities, but also changes in the underlying measurement technique, including changes in the scattering angle, wavelength of light, and channel boundaries. To maintain a continuous *in situ* record, an overlap was maintained when both the new generation and prior generation of instrument were flown in parallel to ensure that, despite the changes in instrument geometries and characteristics, the measurement record remained internally consistent.

This process of instrument succession has continued with the latest generation of instrumentation, the LOPC. The LOPC development period (2016–2019) overlapped with the final flights of the WLPC (2008–2020). Initial comparisons between the LOPC and WLPC were carried out in the laboratory using PSL spheres and atomized ammonium sulfate, size selected using a Scanning Mobility Particle Sizer, diluted to stratospheric concentrations, then verified using a Condensation Particle Counter, see Deshler et al. (2019) for a detailed description. Laboratory comparisons provide a baseline to demonstrate the sizing and counting performance of the new instrument, but as these tests are carried out at surface pressures and temperatures, they do not faithfully represent instrument performance in the stratosphere. Comparing instrument performance in the stratosphere can be most realistically achieved through dual instrument flights, where both the current and replacement instrument are flown simultaneously. Eight such comparison flights were performed from 2017 to 2020. Several of the earlier comparison flights yielded partial comparison profiles from the surface to the upper troposphere, however, none of these flights provided a full comparison as one of the two instruments always exhibited abnormal behavior upon reaching the tropopause. It was finally determined that there was electro-magnetic interference between the two instruments at low pressures. This issue was solved in flight WY932, September 13, 2020, by flying WLPC and LOPC on separate but coordinated balloons, launched less than an hour apart. This provided sufficient separation to avoid interference between instruments, but provided comparable profiles of stratospheric aerosol (Figure 3).

A comparison of the cumulative concentration from LOPC and WLPC for all particles of diameters greater than 0.3, 0.56, 1.2, and 2.34 μm from flight WY932 is shown in Figure 3. There is generally good agreement across the profile, particularly in the stratosphere (above 16 km). LOPC demonstrates a small high bias relative to WLPC near the top of the profile, which is attributed to higher pump efficiency and flow rate at low pressure. There is significant variability and some disagreement in the aerosol concentration for diameters >2.34 μm, possibly due to the low concentrations and Poisson counting statistics compounded by time and spatial differences with the instruments being on different balloons. Figure 4 shows a comparison of WLPC and LOPC size distributions (LOPC re-sampled with 64 bins) for a 500 m vertical average at 18 km, near the peak in the stratospheric aerosol concentration profile. A bimodal lognormal size distribution fit to the WLPC data, using the method described in Deshler et al. (2019), is also shown along with the fitting parameters. The comparison demonstrates that, at all but the largest sizes, the directly measured LOPC size distribution agrees well with the calculated size distribution fit and with the WLPC measurements, obviating the need to fit size distributions prior to calculating extinction and other derived quantities (see Section 4). While the LOPC appears not to capture the second mode in the fitted size distribution, the significant of this is limited due to the significant uncertainty in concentrations of aerosol larger than 2 μm. This discrepancy was already apparent in Figure 3.

Aerosol extinction, a commonly referenced satellite measured aerosol property, can be derived from an integration of an *in situ* measured aerosol size distribution, and thus incorporates the specific response of the instrument from which it is calculated across the range of sizes measured. A comparison of the aerosol extinction profiles for LOPC and WLPC on flight WY932 at 521 and 1,021 nm is shown in Figure 5a. Extinction for each instrument

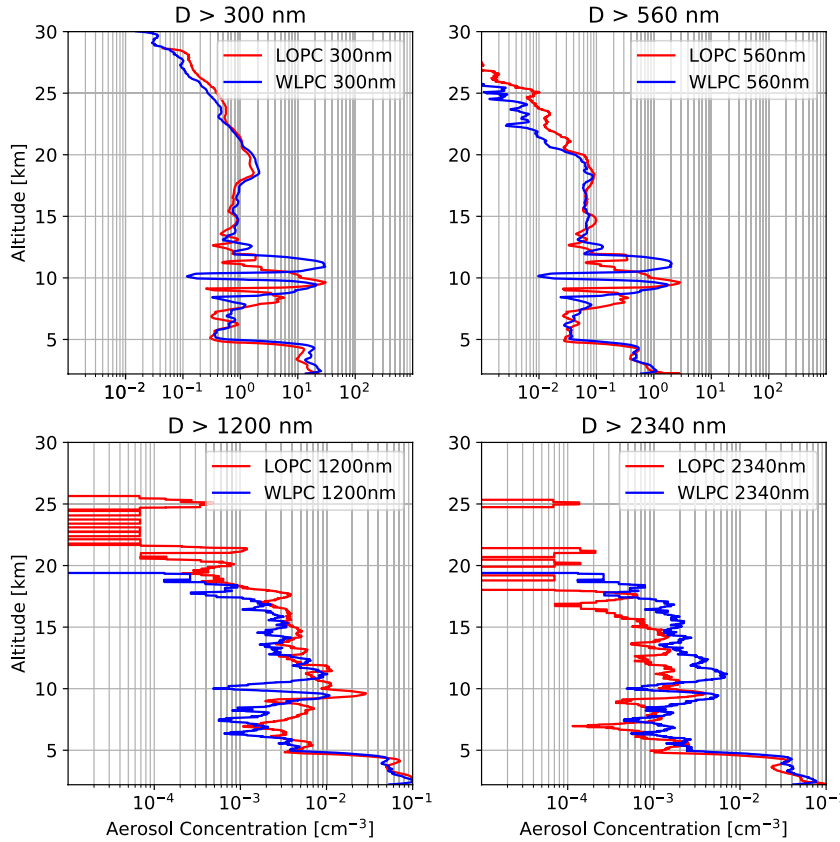

Figure 3. Cumulative aerosol concentration profiles from LASP Optical Particle Counter (LOPC) (red) and Wyoming Laser Particle Counter (WLPC) (blue) from coordinated balloon flights from Laramie, WY on 9/13/2020. The two instruments were flown on separate balloon launched 1 hr appart; differences in the mid troposphere (7–12 km) are attributable to temporal and spatial variations in the cloud field between launches.

is calculated using similar methodologies, described in detail for WLPC in Deshler et al. (2019), and for LOPC in Section 4. The upper tropospheric and stratospheric aerosol extinction profiles generally agree to within the estimated uncertainty, ±40%, for such calculations (Deshler et al., 2003). Below 12 km, spatial and temporal inhomogeneity in the cloud field led to differences in the aerosol profiles. Above 26 km (<20 hPa) differences in sensitivity to the larger particles may be leading to the larger discrepancy there at 1,021 nm. The higher flow rate of the LOPC relative to WLPC increases its sensitivity to larger particles which are more important for the 1,021 nm extinction, while agreement at 521 nm, driven by the smaller particles, is maintained there.

Since 2019, LOPC has been used operationally for aerosol soundings from Boulder, Colorado, performing 4–6 flights per year in coordination with SAGE III/ISS overpasses. These sounding show a very similar vertical aerosol concentration structure to the historical measurement record from WLPC. Figure 6 illustrates this structure using the 0.3 μm aerosol cumulative concentration measurements from both instruments. The 2019–2022 LOPC profiles show higher aerosol concentrations than the mean 2008–2020 WLPC concentrations; however, they agree well with the more recent (darker gray) WLPC profiles. This recent temporal increase in aerosol concentration can be placed in a larger context by extending the 20-yr record of stratospheric aerosol optical depth (sAOD) presented in Kremser et al. (2016).

Figure 7, modeled on a similar figure in Kremser et al. (2016), shows a 25-yr history of sAOD measured *in situ* near 40°N, 105°W, and remotely by SAGE II, SAGE III/ISS, and OSIRIS on ODIN. The calculations of sAOD from the WOPC and WLPC use lognormal size distributions fit to the 8–12 sizes measured by these instruments, whereas sAOD from the LOPC is from direct integration of the 50 sizes publicly reported for these measurments. There is no time filter placed on the satellite data only a latitude and longitude filter. Evident in the figure is the end of the volcanically quiescent period following Pinatubo after the turn of the century, the rather active high latitude volcanism around 2010 leading to higher sAODs, the quasi annual cycle in the satellite sAODs driven

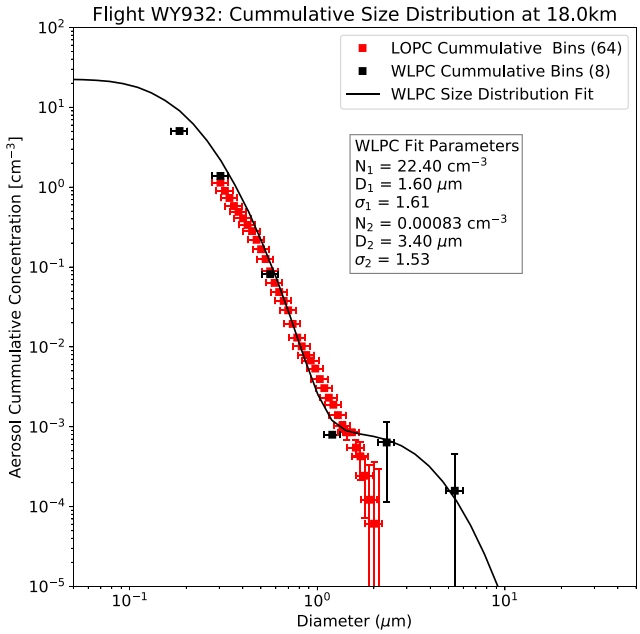

Figure 4. Comparison of Wyoming Laser Particle Counter (WLPC) (black points) and LASP Optical Particle Counter (LOPC) (red points) cumulative size distributions from a 500 m vertical average at 18 km from flight WY932, Laramie WY, on 9/13/2020. A size distribution fit to the WLPC data (black line) is shown along with the number density (N), diameter (D), and distribution width (σ) for each mode. Error bars for diameter represent a 10% uncertainty in sizing and error bars in concentration represent the Poisson counting uncertainty.

by fluctuations in tropopause height, the agreement of the WOPC and WLPC in the overlap period (2008–2015), the general agreement of the *in situ* and satellite sAODs, and the extension of the *in situ* record with the LOPC beginning in 2019. Note in particular the overlap of the sAODs from the WLPC and LOPC late in 2020, the flight shown in Figures 3–5. The red dot of the LOPC is nearly overlain with the black circle of the WLPC. The period since the development of the LOPC (2017 onwards) has been characterized by elevated and highly variable stratospheric aerosol loading, relative to the prior 5 yrs, primarily driven by moderately sized volcanic eruptions as well as injections of smoke into the stratosphere from large wildfires. Overall, the recent comparisons during this dynamic period continue the reasonable agreement of the prior *in situ* and satellite sensors across all the different platforms and instruments.

4. Validation of SAGE III/ISS Measurements of Aerosol Extinction

Along with extending the 50-yr Wyoming record of *in situ* stratospheric aerosol measurements, the other primary motivation for the development of the LOPC is for providing *in situ* validation of satellite measured or derived aerosol properties such as extinction. For comparisons with limb sounding satellites, aerosol extinction is calculated from the aerosol concentration and size distributions. In contrast to the older Wyoming instruments which required fitting an *a priori* size distribution model to a limited number of size bins (Deshler et al., 2019), the high resolution of the LOPC allows for the direct calculation of extinction from the measured size distributions (Figure 4). For this approach, the extinction per particle is calculated for each of the LOPC size bins at each of the relevant satellite wavelengths and is a function of particle diameter and refractive index. The extinction is calculated using the PyMieScatt implementation (Sumlin et al., 2018) of the Bohren and Huffman (2008) form of Lorenz-Mie theory (Mie, 1908). The refractive index is calculated for the relevant wavelengths at the temperature and pressure for each altitude in the profile by assuming a typical stratospheric water vapor mixing ratio of 5 ppmv. The sulfuric acid weight percentage of the aerosol droplets is calculated from Steele and Hamill (1981), the effective refractive index for these droplets is interpolated from the tables of Palmer and Williams (1975), and then the refractive index is corrected to the measured temperature and pressure using the Lorentz-Lorenz relationship, using Luo et al. (1996) for the density of sulfuric acid. The extinction per particle is multiplied by the number of particles in the corresponding bin, then summed across size to yield the total aerosol extinction for each altitude and each satellite wavelength.

Uncertainty in the aerosol extinction derived from the OPC size distribution arises from uncertainties in the underlying measurement of the aerosol size distribution and uncertainties arising from the assumptions inherent in the calculation, primarily the refractive index of the particles. For the underlying LOPC size distributions, a concentration uncertainty of 10% is assumed as the bulk of the stratospheric extinction signal is derived from aerosol with diameters between 0.3 and 1.0 μm and thus concentrations between 0.1 and 1.0 cm^{-3}. The uncertainty in extinction, arising from instrument uncertainty in the determination of aerosol size and number concentration, can be stochastically estimated using a Monte Carlo simulation. For this the aerosol inputs to an extinction algorithm, or any aerosol moment, are varied over their respective range of uncertainties and a population of results is obtained as described in Deshler et al. (2003). Since the LOPC instrumental uncertainties in size and number concentration are similar to the WOPC, used in the simulation completed by Deshler et al. (2003), it seemed reasonable to adopt Deshler et al.'s results for the uncertainty in moment calculations from the LOPC. Thus, the uncertainty in extinction derived from the LOPC is estimated to be ±40% for extinctions between 521 and 1,021 nm. The LOPC has less sensitivity to small particles than the WLPC; however, both analysis and *in situ* comparisons have shown that the impact on the calculated extinction for wavelengths longer than 521 nm is not significant relative to the measurement uncertainty. The per-particle aerosol extinction is a strong function of particle diameter, decreasing exponentially for particles smaller than the wavelength of interest. For the smallest

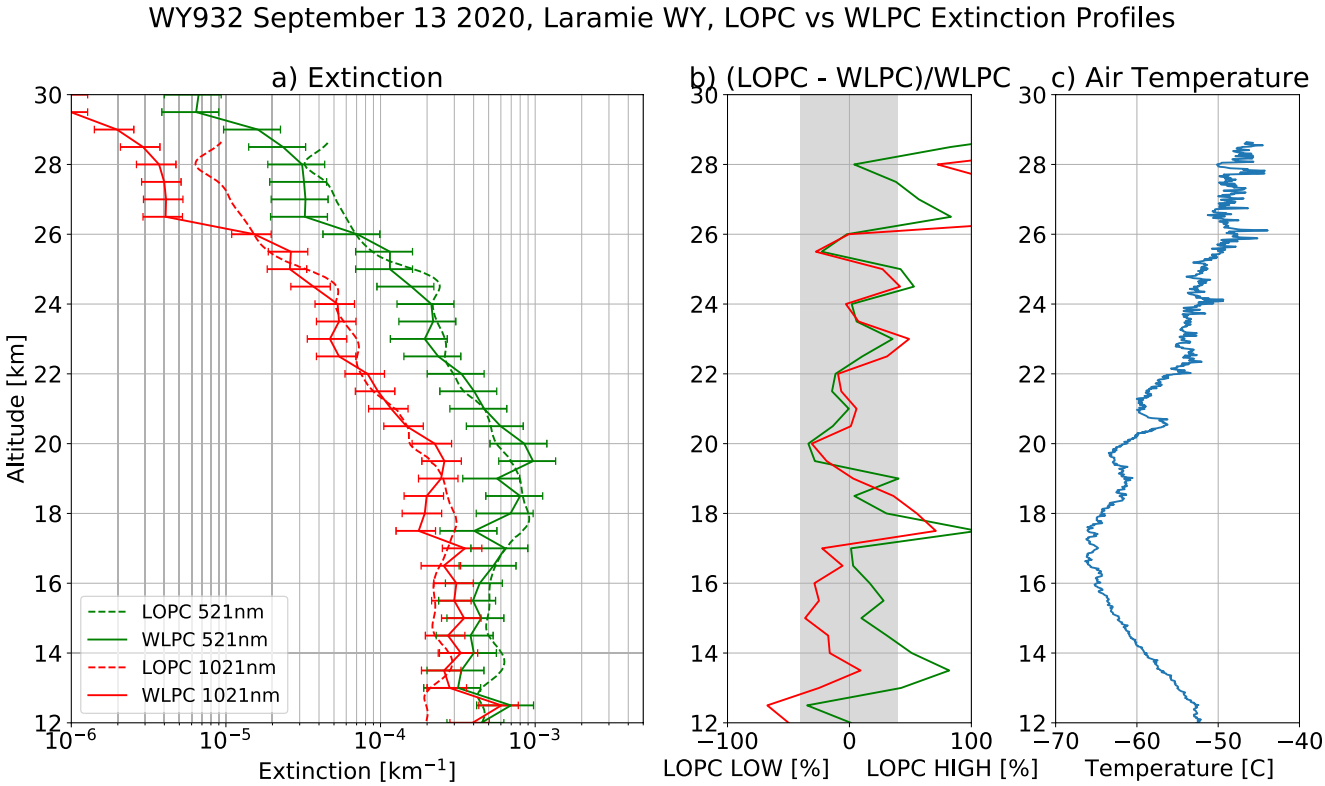

Figure 5. (a) Vertical profiles of extinction at 521 nm (green) and 1,021 nm (red), calculated from Riemann sums of the measured size distributions by LASP Optical Particle Counter (LOPC) (dotted lines and ±40% uncertainty bars) and Wyoming Laser Particle Counter (WLPC) (solid lines). (b) Percent difference of WLPC and LOPC using WLPC as the reference. The gray shading indicates the ±40% uncertainty of the WLPC estimates. (c) Temperature profile.

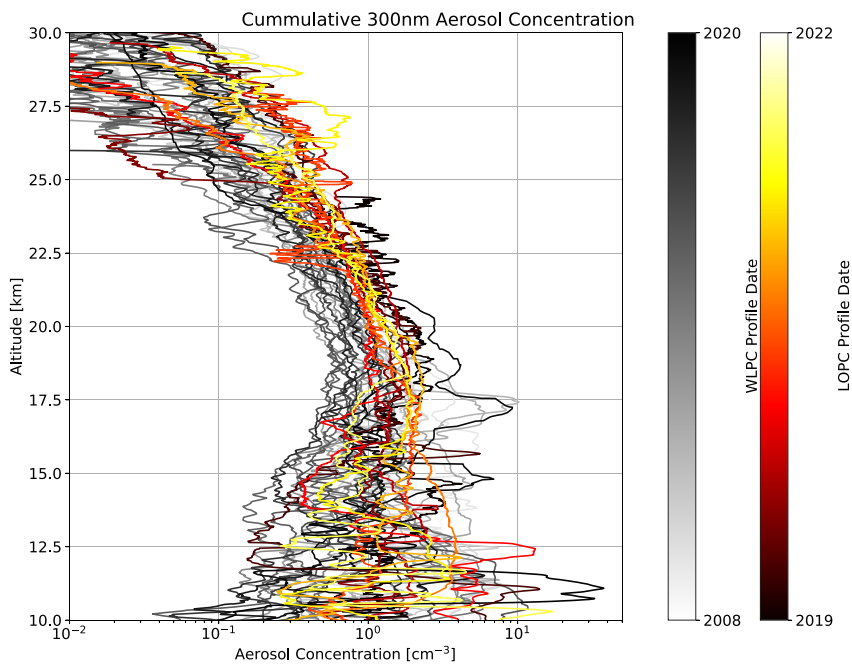

Figure 6. Cumulative aerosol concentration profiles for all particles of diameter larger than 0.3 μm from Wyoming Laser Particle Counter (WLPC) (greys) from 2008 to 2020 and LASP Optical Particle Counter (LOPC) (colors) from 2019 to 2022, color coded by year.

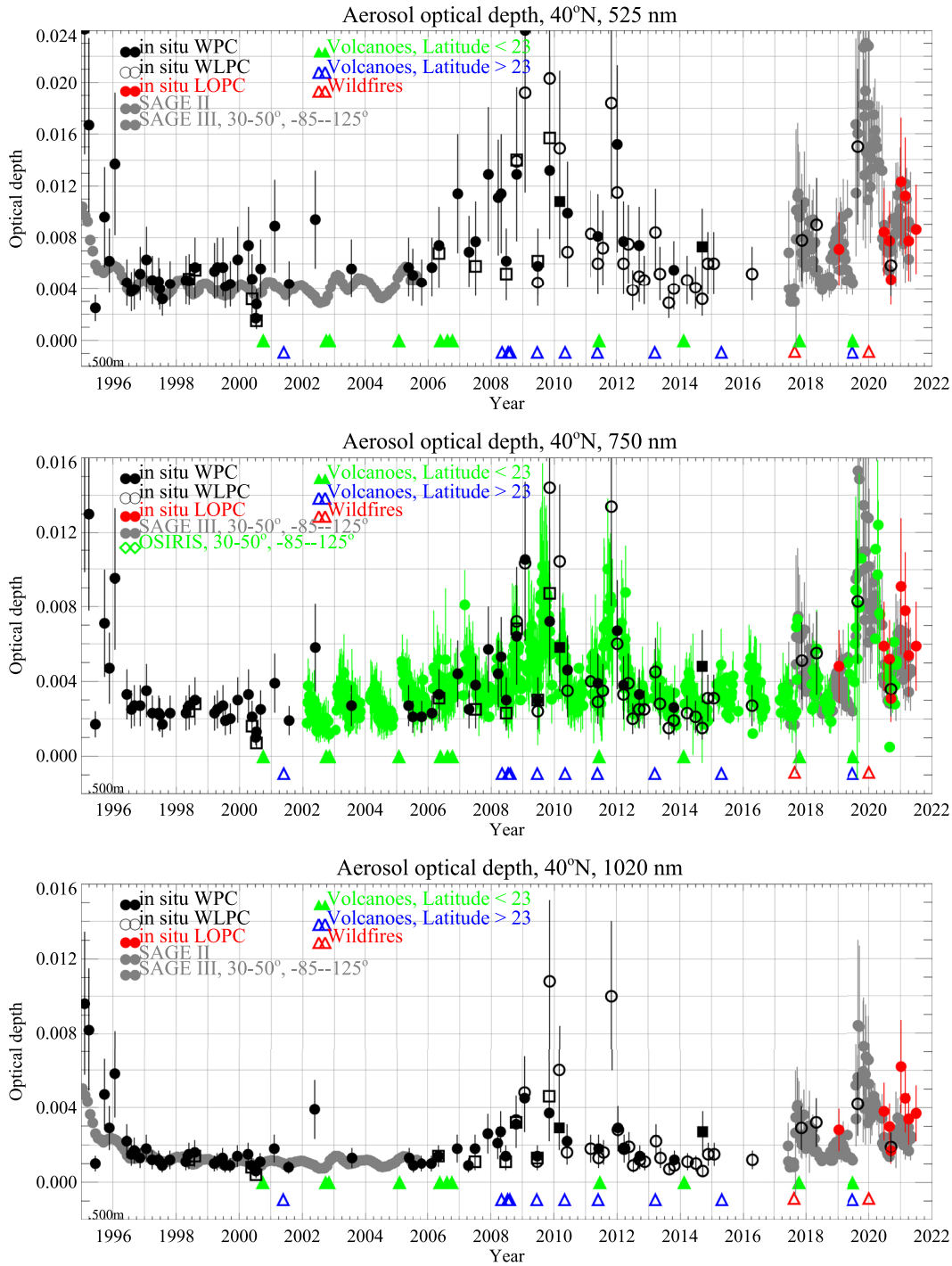

Figure 7. The last 25 years of integrated aerosol extinction from the tropopause to 30 km, stratospheric aerosol optical depth (sAOD), derived from three generations of optical particle counters (OPCs), the Wyoming White Light OPC (WOPC, black dots), the WLPC (black circles), and the LOPC (red dots) in comparison to satellite sAOD including SAGE II (gray dots) from 1984 to 2005, OSIRIS (green dots) on Odin from 2001 to present, and SAGE III/International Space Station (ISS) (gray dots, 521, 755, 1,021 nm) from 2017 onwards. The OSIRIS and SAGE III/ISS data include measurements from 30°N to 50°N and 85°W to 105°W, centered on the *in situ* measurement locations, and are given as monthly averages and standard deviations. On occasion, a second WOPC (open boxes) was flown during the overlap period from the WOPC to the WLPC. The bars on the *in situ* data are ±40%. The tropopauses included in the publicly available SAGE III/ISS and OSIRIS datasets, which are from MERRA, were used for the calculations of sAOD. The SAGE II data are a 5° zonal average centered on 40°N using tropopauses from NCEP. The OPC tropopauses are the locally measured thermal tropopause. The timing of volcanic eruptions are shown at latitudes <23° with green triangles, and at latitudes >23° with blue triangles along the bottom of each panel. Recent significant wildfire events are indicated with red triangles.

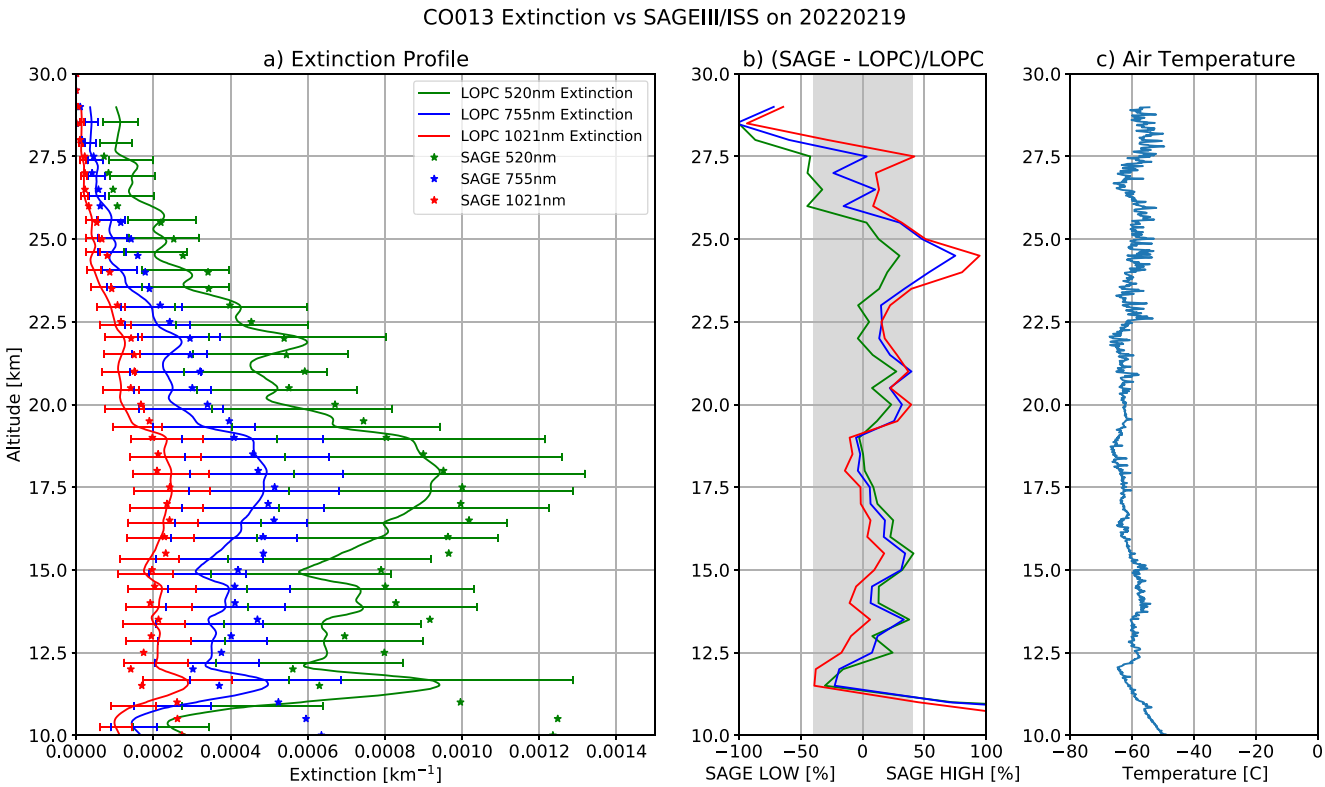

Figure 8. A profile-to-profile comparison between LASP Optical Particle Counter (LOPC)-derived aerosol extinction and a nearby SAGE III/International Space Station (ISS) profile showing (a) the 520 nm (green), 755 nm (blue), and 1,021 nm (red) extinction profile; (b) the percentage difference between the extinction profiles using LOPC as the reference; the gray box indicates the 40% uncertainty in OPC extinction; and (c) the temperature profile from the balloon sounding, indicating a thermal tropopause at 12.2 km.

particles that LOPC detects (albeit with a counting efficiency <1.0) with a diameter of 0.25 μm, the per-particle extinction at 521 nm is 1.5 orders of magnitude smaller than the extinction of a 0.52 μm particle, thus the extinction at 521 nm attributable to aerosol not detected by the LOPC is a small contribution. In practice, comparing the extinction calculated from WLPC (minimum size 0.18 μm) with the extinction calculated from LOPC show extinction agreements well within the 40% uncertainty, and no systematic low bias in LOPC calculated extinction. However, care should be taken in calculating extinction at shorter wavelengths close to the minimum detectable size of the instrument.

4.1. Comparisons With SAGE III/ISS

From 2017 to the present, 16 aerosol soundings were performed in coordination with nearby SAGE III/ISS solar occultations, 12 flights using LOPC, three using WLPC, and one using both WLPC and LOPC. The balloon soundings were planned to conform with a match criterion of within ±24 hr, ±5° of latitude, ±10° of longitude of a SAGE III/ISS solar occultation that was likely to yield a successful aerosol extinction retrieval. Not all the balloon soundings provided a useful comparison with SAGE III/ISS due to instrument and balloon problems; however, 12 successful matched profiles have been collected. Comparisons between OPC-derived aerosol extinction and SAGE III/ISS extinction are performed on a profile-by-profile basis with an example of an aerosol extinction profile comparison between SAGE III/ISS and LOPC shown in Figure 8. This comparison is based on a February 2022 balloon flight from Boulder, CO. The closest corresponding SAGE III/ISS profile is 370 km NW of the launch location and 2 hr prior to the balloon launch. Extinction at the two SAGE wavelengths shown was calculated using the methodology described previously for LOPC, that is, using directly the LOPC's 450 aerosol channels, without fitting a size distribution. This profile is typical of the comparisons collected so far, and illustrates several salient features.

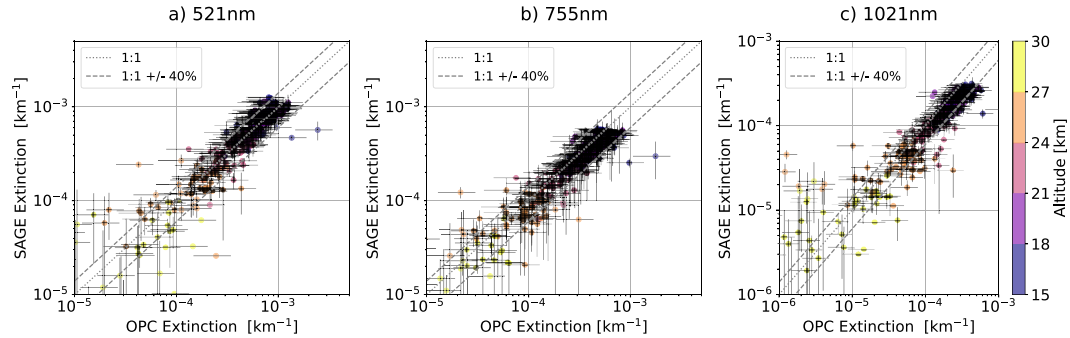

Figure 9. Scatter plots of LASP Optical Particle Counter (LOPC)-derived extinctions and SAGE III measured extinctions at (a) 521, (b) 755, and (c) 1,021 nm for all LOPC measurements which met the match criteria. The LOPC estimates include the instrumental uncertainty of ±40%. The corresponding SAGE III measurements are the average and standard deviations of all SAGE III measurements within ±48 hr, ±10° of latitude, ±20° of longitude, twice the match criteria used when identifying a day for an LOPC flight. The data are color coded in 3 km altitude bins. A 1:1 line as well as lines within ±40% of the 1:1 line are provided as a guide.

Above the thermal tropopause (in this example around 12.2 km) LOPC and SAGE largely agree within the 40% uncertainty prescribed to OPC-derived extinction. At and below the tropopause, the agreement between LOPC and SAGE III/ISS extinction decreases. Tropospheric aerosol extinction from SAGE III/ISS that was measured 370 km away is expected to have little correlation with the *in situ* profiles, particularly on days with cloud cover, and thus without tighter match criteria; only measurements above the tropopause yield meaningful comparisons. Features in the aerosol profile with vertical scales near the 0.5 km reported vertical resolution of SAGE III/ISS are not fully captured in the SAGE III/ISS aerosol extinction profiles, leading to a low bias in the satellite-derived aerosol extinction near the peak in the stratospheric aerosol column near the tropopause at 12.3 km. This bias is more evident in profiles with more distinct structure, such as in the presence of recent volcanic or wildfire smoke aerosol layers, and may be exacerbated by the presence of non-sulfate aerosol with different refractive indices as well as a shift to smaller particle sizes that are not well captured by the LOPC. Finally, above 26 km, where aerosol concentrations are low and extinctions are $<2 \times 10^{-4}$ km^{-1} there is increasing divergence between SAGE III/ISS and the *in situ* measurements; this divergence is evident in the majority of profile-to-profile comparisons.

Figure 9 compares the 12 LOPC flights that met the match criteria specified above, with averages of the coincident SAGE III/ISS measurements that are within twice the match criteria. The error bars on the SAGE data are the standard deviation of all the satellite measurements that met the expanded match criteria and provide an estimate of temporal and spatial inhomogeneity and not SAGE III/ISS instrumental error, whereas the error bars on the LOPC extinction axis (x) are representative of instrumental uncertainty in the LOPC-derived extinction. For the 521 and 755 nm aerosol extinction (Figures 9a and 9b), the SAGE III/ISS and LOPC measurements are well correlated (Pearson's correlation $r = 0.85$), cluster around the 1:1 line, indicating no systematic bias between the measurements, and the majority of the points lie between the ±40% lines, suggesting a majority of measurements are in agreement within the uncertainty of the LOPC estimates. For altitudes near or below typical tropopause heights (blue points), there are a few outliers, representing increased spatial inhomogeneity at or below the tropopauses. Decreased agreement is also seen above 26.5 km, yellow points, and extinctions below 10^{-4} km^{-1}, however in this case the points predominantly fall below the 1:1 line, indicating SAGE III/ISS aerosol extinctions are lower than the *in situ* measurements. This is a region where aerosol concentrations are generally limited to particles <0.8 μm diameter at concentrations near 0.01 cm^{-3} which is still adequate to provide a reasonable extinction estimate, and presumably also adequate for a reasonable satellite measurement. This discrepancy is consistent with analysis that suggests that the SAGE III/ISS aerosol retrieval algorithm may have an altitude-dependent low bias in the 500–600 nm region that results in a 20%–30% underestimation of extinction (Wang et al., 2020).

An analogous scatter plot for 1,021 nm aerosol extinction is shown in Figure 9c. The comparison again shows a high level of correlation between the measurements ($r = 0.84$); however, the majority of comparisons at extinctions greater than 10^{-5} km^{-1} fall below the one to one line, indicating a low bias in SAGE III/ISS relative to the LOPC. This bias is broadly consistent with previous comparisons between OPC-derived extinction and satellite-derived extinction measurements, including SAGE II (Deshler et al., 2019), and may be further amplified

by the increased sensitivity of the LOPC to large particles in the stratosphere relative to prior generations of OPCs. However, the majority of SAGE III/ISS extinction measurements are still within the 40% error margin of the LOPC-derived extinction. Similar scatter plots for all the SAGE aerosol wavelengths show equivalent levels of correlation, and generally increasing low bias in SAGE III/ISS with increasing wavelength.

5. Conclusion

The LOPC is a new instrument developed to make balloon-borne *in situ* aerosol size distribution measurements with a size and concentration range overlapping the previous instruments flown from Laramie, Wyoming, including sensitivity to super micron particles at low concentrations. Both laboratory and in-flight evaluation of the new LOPC instrument and the prior generation of Wyoming OPCs (WLPC) yielded aerosol extinction profiles that agreed within measurement uncertainty. A comparison of aerosol concentration profiles between the LOPC and the last decade of WLPC measurements shows that the LOPC measurements are within the range of WLPC measurements and are capturing the increase in stratospheric aerosol concentrations that has been observed since 2019. Initial comparisons of stratospheric aerosol extinction derived from LOPC measurements of aerosol size distributions, and extinction profiles from SAGE III/ISS, indicate generally good agreement on a profile-by-profile basis. For 521, 755, and 1,021 nm extinction the LOPC measurements are tightly correlated with matched SAGE III/ISS profiles and in all cases the majority of altitude by altitude comparisons are within the margin of uncertainty of the LOPC-derived extinction. There is some evidence for a low bias in the SAGE 1,021 nm channel relative to LOPC, but this is still within the margin of error and will require further work to diagnose. Increased variance between SAGE III/ISS and the LOPC is observed near and below the tropopause, likely due to spatial inhomogeneity and above 25 km when extinctions are below 5×10^{-5} km^{-1}. Furthermore, time series comparisons of sAOD form OPCs and satellites suggest similar agreement between SAGE III/ISS and LOPC as was seen between SAGE II and prior generations of Wyoming OPCs, indicating that both SAGE III/ISS and LOPC will continue to produce an accurate record of stratospheric aerosol properties. This study is ongoing, and these initial results suggest that the SAGE III/ISS aerosol extinction products meet or exceed the level of agreement established between prior *in situ* and satellite comparisons. Further coordinated measurements that are currently in progress will allow for more rigorous comparisons to be made.

Data Availability Statement

The LOPC and WLPC data are available in the data repository at the University of Wyoming Libraries (Deshler & Kalnajs, 2022). The SAGE data used in these comparisons is available from the NASA Atmospheric Science Data Center (SAGE Science Team, 2021). Figures were generated using Matplotib version 3.6.2 (Caswell et al., 2022).

Acknowledgments
The development of the LOPC instrument was funded by the National Science Foundation under Award 1619632. Continued sounding using the instrument and SAGE III/ISS validation efforts are funded by the National Aeronautics and Space Agency under awards 80NSSC18K0709 and 80NSSC21K1198. Gratitude is extended to Landon Rieger for help with bringing the OSIRIS data up to date for Figure 7.

References

Barnes, J. E., & Hofmann, D. J. (1997). Lidar measurements of stratospheric aerosol over Mauna Loa Observatory. *Geophysical Research Letters*, *24*(15), 1923–1926. https://doi.org/10.1029/97GL01943

Bigg, E. K., Ono, A., & Thompson, W. J. (1970). Aerosols at altitudes between 20 and 37 km. *Tellus*, *22*(5), 550–563. https://doi.org/10.1111/j.2153-3490.1970.tb00522.x

Bohren, C. F., & Huffman, D. R. (2008). *Absorption and scattering of light by small particles*. John Wiley & Sons.

Bourassa, A. E., Degenstein, D. A., Gattinger, R. L., & Llewellyn, E. J. (2007). Stratospheric aerosol retrieval with optical spectrograph and infrared imaging system limb scatter measurements. *Journal of Geophysical Research (Atmospheres)*, *112*(D10), D10217. https://doi.org/10.1029/2006JD008079

Caswell, T. A., Lee, A., Droettboom, M., De Andrade, E. S., Hoffmann, T., Klymak, J., et al. (2022). *matplotlib/matplotlib: REL: v3.6.2 (Version v3.6.2)*. Zenodo. https://doi.org/10.5281/ZENODO.7275322

Deshler, T., Anderson-Sprecher, R., Jäger, H., Barnes, J., Hofmann, D. J., Clemesha, B., et al. (2006). Trends in the nonvolcanic component of stratospheric aerosol over the period 1971–2004. *Journal of Geophysical Research*, *111*(D1), D01201. https://doi.org/10.1029/2005JD006089

Deshler, T., Hervig, M. E., Hofmann, D. J., Rosen, J. M., & Liley, J. B. (2003). Thirty years of in situ stratospheric aerosol size distribution measurements from Laramie, Wyoming (41°N), using balloon-borne instruments. *Journal of Geophysical Research*, *108*(D5), 4167. https://doi.org/10.1029/2002JD002514

Deshler, T., & Kalnajs, L. E. (2022). University of Wyoming stratospheric aerosol measurements | Mid latitudes [Dataset]. https://doi.org/10.15786/21534894

Deshler, T., Luo, B., Kovilakam, M., Peter, T., & Kalnajs, L. E. (2019). Retrieval of aerosol size distributions from in situ particle counter measurements: Instrument counting efficiency and comparisons with satellite measurements. *Journal of Geophysical Research: Atmospheres*, *124*(9), 5058–5087. https://doi.org/10.1029/2018JD029558

Hervig, M., & Deshler, T. (2002). Evaluation of aerosol measurements from SAGE II, HALOE, and balloonborne optical particle counters. *Journal of Geophysical Research*, *107*(D3), AAC3-1–AAC3-12. https://doi.org/10.1029/2001JD000703

Hofmann, D. J., & Deshler, T. (1991). Stratospheric cloud observations during formation of the Antarctic ozone hole in 1989. *Journal of Geophysical Research*, *96*(D2), 2897–2912. https://doi.org/10.1029/90JD02494

Hofmann, D. J., & Rosen, J. M. (1981). On the background stratospheric aerosol layer. *Journal of the Atmospheric Sciences*, *38*(1), 168–181. https://doi.org/10.1175/1520-0469(1981)038<0168:OTBSAL>2.0.CO;2

Hofmann, D. J., & Rosen, J. M. (1987). On the prolonged lifetime of the El Chichón sulfuric acid aerosol cloud. *Journal of Geophysical Research*, *92*(D8), 9825–9830. https://doi.org/10.1029/JD092iD08p09825

Hofmann, D. J., Rosen, J. M., Pepin, T. J., & Pinnick, R. G. (1975). Stratospheric aerosol measurements I: Time variations at northern midlatitudes. *Journal of the Atmospheric Sciences*, *32*(7), 1446–1456. https://doi.org/10.1175/1520-0469(1975)032<1446:SAMITV>2.0.CO;2

Jäger, H. (2005). Long-term record of lidar observations of the stratospheric aerosol layer at Garmisch-Partenkirchen. *Journal of Geophysical Research*, *110*(D8), D08106. https://doi.org/10.1029/2004JD005506

Junge, C. E., Chagnon, C. W., & Manson, J. E. (1961). Stratospheric Aerosols. *Journal of Meteorology*, *18*(1), 81–108. https://doi.org/10.1175/1520-0469(1961)018<0081:SA>2.0.CO;2

Junge, C. E., & Manson, J. E. (1961). Stratospheric aerosol studies. *Journal of Geophysical Research (1896–1977)*, *66*(7), 2163–2182. https://doi.org/10.1029/JZ066i007p02163

Kremser, S., Thomason, L. W., von Hobe, M., Hermann, M., Deshler, T., Timmreck, C., et al. (2016). Stratospheric aerosol—Observations, processes, and impact on climate. *Reviews of Geophysics*, *54*(2), 278–335. https://doi.org/10.1002/2015RG000511

Llewellyn, E. J., Lloyd, N. D., Degenstein, D. A., Gattinger, R. L., Petelina, S. V., Bourassa, A. E., et al. (2004). The OSIRIS instrument on the Odin spacecraft. *Canadian Journal of Physics*, *82*(6), 411–422. https://doi.org/10.1139/p04-005

Luo, B., Krieger, U. K., & Peter, T. (1996). Densities and refractive indices of $H_2SO_4/HNO_3/H_2O$ solutions to stratospheric temperatures. *Geophysical Research Letters*, *23*(25), 3707–3710. https://doi.org/10.1029/96GL03581

Ma, X., Lu, J. Q., Brock, R. S., Jacobs, K. M., Yang, P., & Hu, X.-H. (2003). Determination of complex refractive index of polystyrene microspheres from 370 to 1610 nm. *Physics in Medicine and Biology*, *48*(24), 4165–4172. https://doi.org/10.1088/0031-9155/48/24/013

Massie, S. T., Gille, J. C., Edwards, D. P., Bailey, P. L., Lyjak, L. V., Craig, C. A., et al. (1996). Validation studies using multiwavelength Cryogenic Limb Array Etalon Spectrometer (CLAES) observations of stratospheric aerosol. *Journal of Geophysical Research*, *101*(D6), 9757–9773. https://doi.org/10.1029/95JD03225

McCormick, M. P., Hamill, P., Pepin, T. J., Chu, W. P., Swissler, T. J., & McMaster, L. R. (1979). Satellite studies of the stratospheric aerosol. *Bulletin of the American Meteorological Society*, *60*(9), 1038–1047. https://doi.org/10.1175/1520-0477(1979)060<1038:SSOTSA>2.0.CO;2

Mie, G. (1908). Beiträge zur Optik trüber Medien, speziell kolloidaler Metallösungen. *Annalen der Physik*, *330*(3), 377–445. https://doi.org/10.1002/andp.19083300302

Palmer, K. F., & Williams, D. (1975). Optical constants of sulfuric acid; application to the clouds of venus? *Applied Optics*, *14*(1), 208–219. https://doi.org/10.1364/AO.14.000208

Pinnick, R. G., Rosen, J. M., & Hofmann, D. J. (1973). Measured light-scattering properties of individual aerosol particles compared to Mie scattering theory. *Applied Optics*, *12*(1), 37–41. https://doi.org/10.1364/AO.12.000037

Reeves, J., Wilson, J. C., Brock, C., & Bui, T. (2008). Comparison of aerosol extinction coefficients, surface area density, and volume density from SAGE II and in situ aircraft measurements. *Journal of Geophysical Research*, *113*(D10), D10202. https://doi.org/10.1029/2007JD009357

Rosen, J. M. (1964). The vertical distribution of dust to 30 kilometers. *Journal of Geophysical Research (1896–1977)*, *69*(21), 4673–4676. https://doi.org/10.1029/JZ069i021p04673

Russell, P. B., McCormick, M. P., Swissler, T. J., Chu, W. P., Livingston, J. M., Fuller, W. H., et al. (1981). Satellite and correlative measurements of the stratospheric aerosol. II: Comparison of measurements made by SAM II, dustsondes and an airborne lidar. *Journal of the Atmospheric Sciences*, *38*(6), 1295–1312. https://doi.org/10.1175/1520-0469(1981)038<1295:SACMOT>2.0.CO;2

Russell, P. B., McCormick, M. P., Swissler, T. J., Rosen, J. M., Hofmann, D. J., & McMaster, L. R. (1984). Satellite and correlative measurements of the stratospheric aerosol. III: Comparison of measurements by SAM II, SAGE, dustsondes, filters, impactors and lidar. *Journal of the Atmospheric Sciences*, *41*(11), 1791–1800. https://doi.org/10.1175/1520-0469(1984)041<1791:SACMOT>2.0.CO;2

SAGE Science Team. (2021). SAGE III/ISS L2 monthly solar event species profiles (NetCDF) V052 [Dataset]. NASA Langley Atmospheric Science Data Center DAAC. https://doi.org/10.5067/ISS/SAGEIII/SOLAR_NETCDF4_L2-V5.2

Steele, H. M., & Hamill, P. (1981). Effects of temperature and humidity on the growth and optical properties of sulphuric acid—Water droplets in the stratosphere. *Journal of Aerosol Science*, *12*(6), 517–528. https://doi.org/10.1016/0021-8502(81)90054-9

Sumlin, B. J., Heinson, W. R., & Chakrabarty, R. K. (2018). Retrieving the aerosol complex refractive index using PyMieScatt: A Mie computational package with visualization capabilities. *Journal of Quantitative Spectroscopy and Radiative Transfer*, *205*, 127–134. https://doi.org/10.1016/j.jqsrt.2017.10.012

Thomason, L. W., Ernest, N., Millán, L., Rieger, L., Bourassa, A., Vernier, J.-P., et al. (2018). A global space-based stratospheric aerosol climatology: 1979–2016. *Earth System Science Data*, *10*(1), 469–492. https://doi.org/10.5194/essd-10-469-2018

Vernier, J.-P., Pommereau, J.-P., Thomason, L. W., Pelon, J., Garnier, A., Deshler, T., et al. (2011). Overshooting of clean tropospheric air in the tropical lower stratosphere as seen by the CALIPSO lidar. *Atmospheric Chemistry and Physics*, *11*(18), 9683–9696. https://doi.org/10.5194/acp-11-9683-2011

Wang, H. J. R., Damadeo, R., Flittner, D., Kramarova, N., Taha, G., Davis, S., et al. (2020). Validation of SAGE III/ISS solar occultation ozone products with correlative satellite and ground-based measurements. *Journal of Geophysical Research: Atmospheres*, *125*(11), e2020JD032430. https://doi.org/10.1029/2020JD032430

Ward, S. M., Deshler, T., & Hertzog, A. (2014). Quasi-Lagrangian measurements of nitric acid trihydrate formation over Antarctica. *Journal of Geophysical Research: Atmospheres*, *119*(1), 245–258. https://doi.org/10.1002/2013JD020326